PROCEEDINGS OF SPIE

SPIEDigitalLibrary.org/conference-proceedings-of-spie

Tunable 1060nm VCSEL co-packaged with pump and SOA for OCT and LiDAR

Bart Johnson, Walid Atia, Seungbum Woo, Carlos Melendez, Mark Kuznetsov, et al.

Bart Johnson, Walid Atia, Seungbum Woo, Carlos Melendez, Mark Kuznetsov, Tim Ford, Nate Kemp, Joey Jabbour, Ed Mallon, Peter Whitney, "Tunable 1060nm VCSEL co-packaged with pump and SOA for OCT and LiDAR," Proc. SPIE 10867, Optical Coherence Tomography and Coherence Domain Optical Methods in Biomedicine XXIII, 1086706 (22 February 2019); doi: 10.1117/12.2510395

Event: SPIE BiOS, 2019, San Francisco, California, United States

Tunable 1060 nm VCSEL co-packaged with pump and SOA for OCT and LiDAR

Bart Johnson, Walid Atia, Seungbum Woo, Carlos Melendez, Mark Kuznetsov, Tim Ford, Nate Kemp, Joey Jabbour, Ed Mallon, and Peter Whitney

Axsun Technologies, Billerica, MA, USA

ABSTRACT

A 1060 nm optically pumped tunable VCSEL was formed from an InGaAs/AlGaAs/GaAs half-VCSEL bonded to a MEMS movable mirror on a silicon substrate. The VCSEL was co-packaged in a 14-pin butterfly module with an 825 nm pump laser and a 1060 nm semiconductor optical amplifier. The co-packaged device exhibited shot-noise-limited sensitivity with up to 50 mW output power and 75 nm tunability. Ophthalmic OCT, especially whole-eye imaging and ocular biometry, is considered the primary application of this device. However, we have also investigated LiDAR to greater than 10 meter ranges with non-mechanical beam steering through angular diffraction from a grating. A new generation of photonic integrated circuit LiDARs work this way and we have investigated the depth resolution limitations due to time dispersion from the grating. Distributed fiber temperature sensing was also demonstrated.

Keywords: Tunable VCSEL, Swept laser, Swept source, OCT, Optical Coherence Tomography, LiDAR, Distributed fiber sensing

1. INTRODUCTION

MEMS tunable VCSELs have been available at 1060, 1310, and 1550 nm for a number of years. Many of these VCSELs are optically pumped and require amplification to achieve required optical powers. This requires assembly of a number of optical components to make the VCSEL into a useful source. While impressive ophthalmic OCT studies at 1060 nm have been performed,[1] the sources have a limited amount of packaging integration.[2] An exception to the rule is a Coretek, Inc. 1550 nm VCSEL that was co-packaged with a pump, SOA and numerous other optical elements.[3] A version of that module was used in the first VCSEL OCT imaging experiments at MIT in 2005.[4] We report here a 1060 nm tunable VCSEL formed from an InGaAs/AlGaAs/GaAs half-VCSEL bonded to a MEMS movable mirror on a silicon substrate. This optically-pumped VCSEL is co-packaged in a 14-pin butterfly module (Fig. 1) with its pump laser and a SOA to boost its mW-level powers up to levels exceeding 50 mW. OCT system experiments demonstrated shot-noise-limited sensitivity.

Bart Johnson: bjohnson@axsun.com

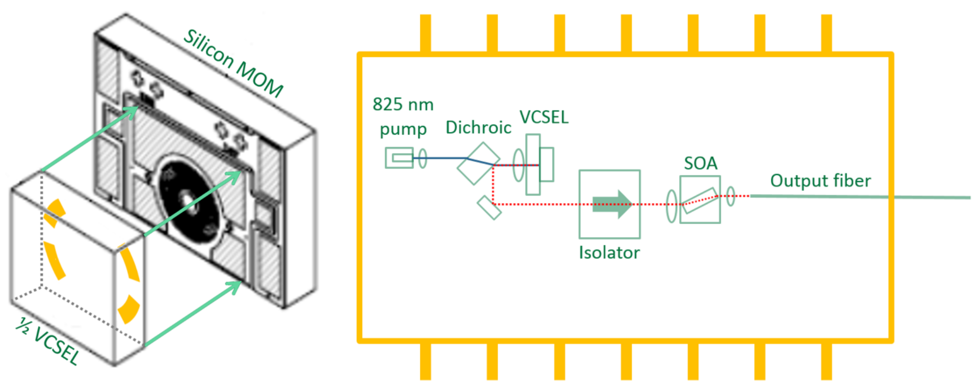

Figure 1. (Left) Die bonding process to create the VCSEL. (Right) Copackaging in a 14-pin butterfly module of VCSEL with pump laser and SOA.

Optical Coherence Tomography and Coherence Domain Optical Methods in Biomedicine XXIII
edited by James G. Fujimoto, Joseph A. Izatt, Proc. of SPIE Vol. 10867, 1086706

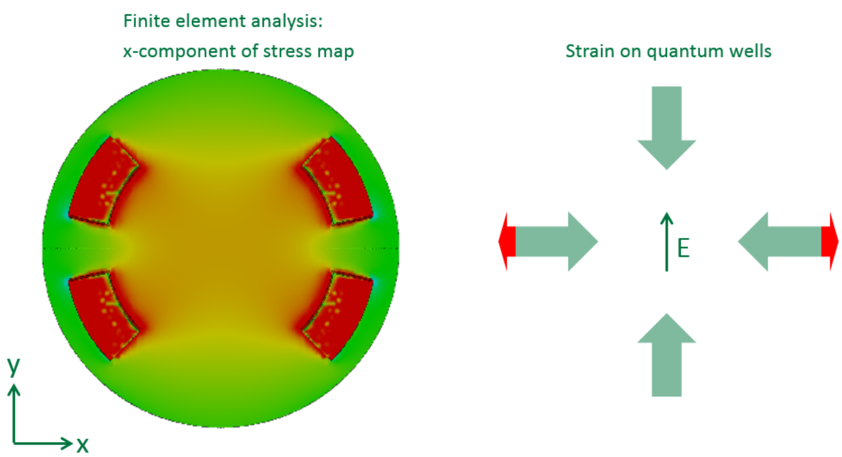

Figure 2. (Left) The finite-element x-stress map shows the thermal expansion stress between the silicon and GaAs wafers with asymmetric bond pad spacings. (Right) The strain on the active layers is a combination of built-in crystal strain (green) and wafer bonding strain (red), leading to a y-polarization of the laser radiation.

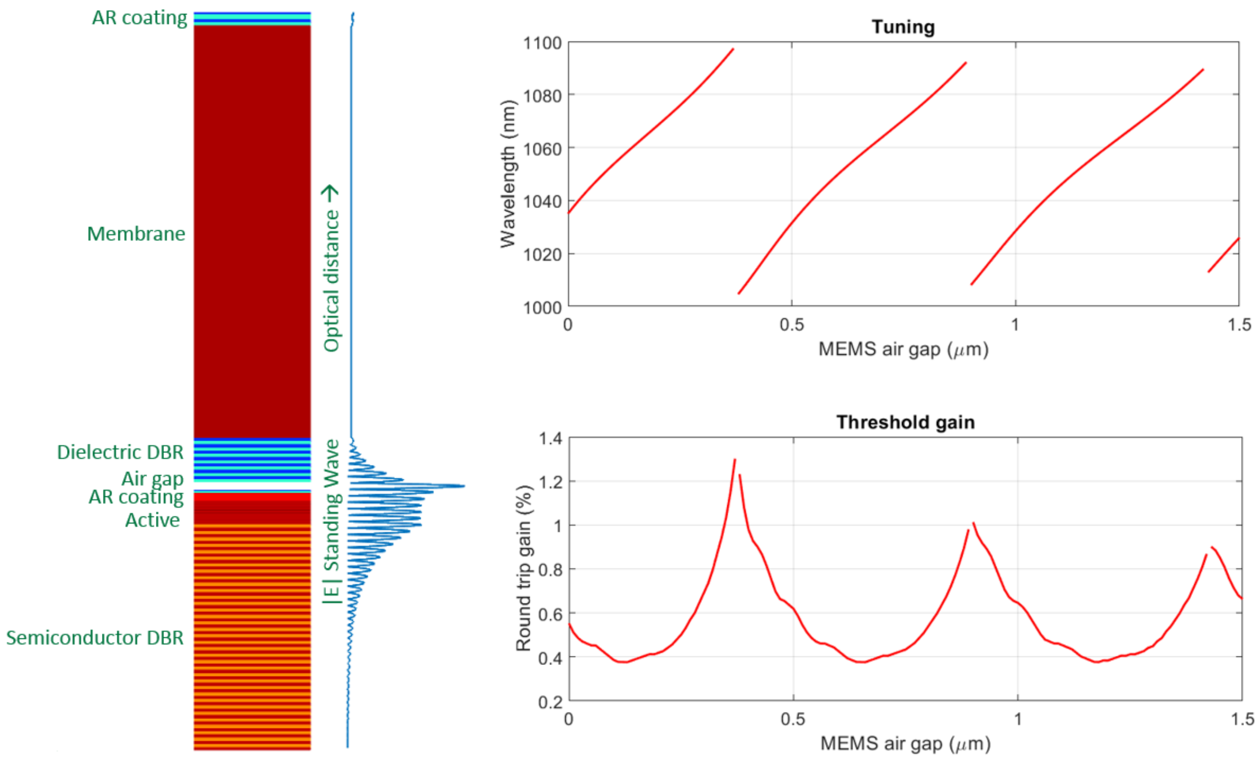

Figure 3. Calculations of VCSEL tuning range. The VCSEL structure is color coded by refractive index at the left with |E|, the electric field standing wave plotted alongside. The model allows calculation of the wavelength and threshold gain as the MEMS air gap is varied.

2. DEVICE AND PACKAGING

The VCSEL is formed by thermocompression bonding a 1/2-VCSEL (Multi-quantum-well gain medium and AlGaAs/GaAs DBR on a GaAs substrate) to a mirror on membrane (MOM), which is an electrostatically movable MEMS mirror on a silicon substrate.[5] Polarization is controlled by asymmetric strain of the active layer.[6] The die bonding process occurs at high temperature and the different thermal contractions of the GaAs and silicon substrates causes the strain once cooled, as shown in Fig. 2. The tunable VCSEL structure consists of 100+ material layers as depicted on the left side of Fig. 3. Multilayer stack field simulations[7] allow calculation of the wavelength and threshold gain. These calculations work very well and are important for increasing the tuning range to the limits of the technology. The limiting factor for tunability is the bandwidth of the semiconductor DBR, which has relatively low index contrast. On the other hand, this mirror is grown into the crystal promoting a very reliable monolithic structure. Other mirror technologies, such as GaAs/AlAs-oxidized mirrors,[8] dielectric mirrors, and metal/dielectric hybrid mirrors have been investigated or proposed. These methods involve removing or modifying material near the very thin quantum well active layers and may be of concern on reliability grounds. While these important technologies are under development, it is also of critical interest to understand the limits of the monolithic approach.

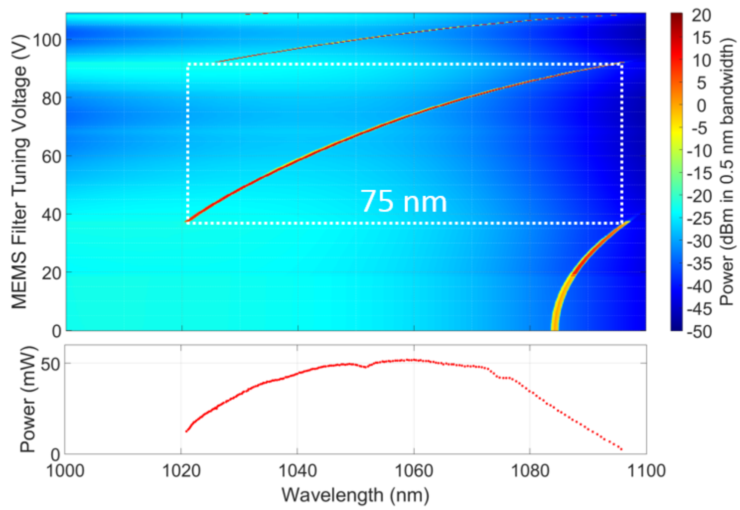

Figure 4. Static tuning of the co-packaged VCSEL/pump/SOA. The tuning range on the second Fabry-Perot order is 75 nm. The peak power exceeds 50 mW.

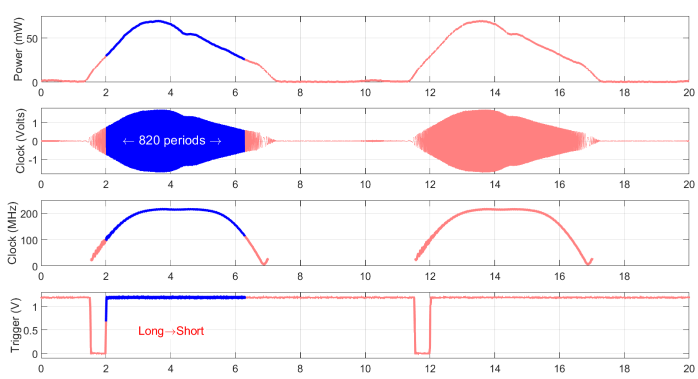

Figure 5. Dynamic tuning of a VCSEL at a 100 kHz sweep rate. The clock is cut for a 3.7 mm Nyquist depth. A full data-collection sweep (shown in blue) is 820 clock cycles long.

The VCSEL was packaged in a 14-pin butterfly module with an 825 nm pump laser, a dichroic mirror, optical isolator, and semiconductor optical amplifier (SOA). Compared to a separated pump, VCSEL, isolator, and SOA, co-packaging has advantages in cost, polarization control, and elimination of parasitic reflections that impair system performance.

Static and dynamic tuning data for the laser system are shown in Figs. 4 and 5. On the second tuning order of the VCSEL Fabry-Perot cavity, a 75 nm tuning range was obtained (Fig. 4). During dynamic tuning the retrace was blanked by shutting off the SOA (Fig. 5) and the average power was 25 mW.

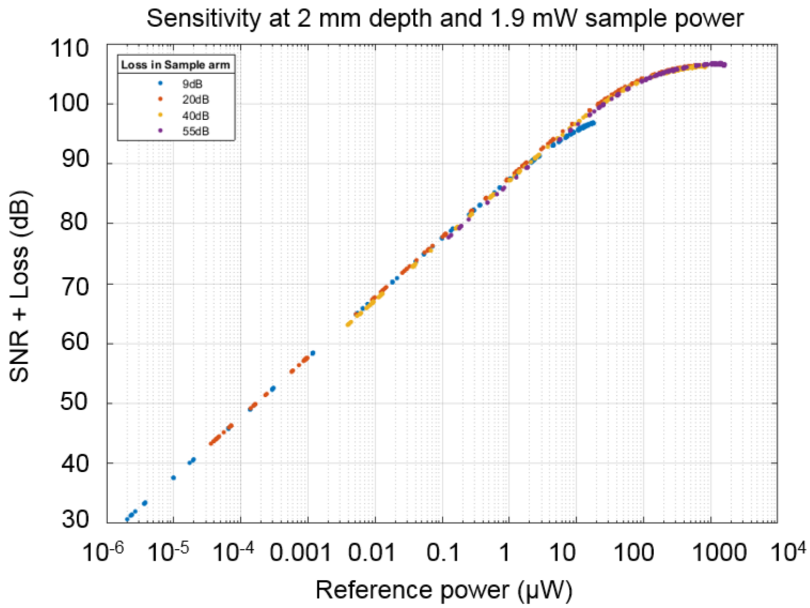

Figure 6. Co-packaged VCSEL/pump/SOA sensitivity measurement at a 40 kHz sweep rate by direct hardware clocking. A shot-noise-limited sensitivity was achieved.

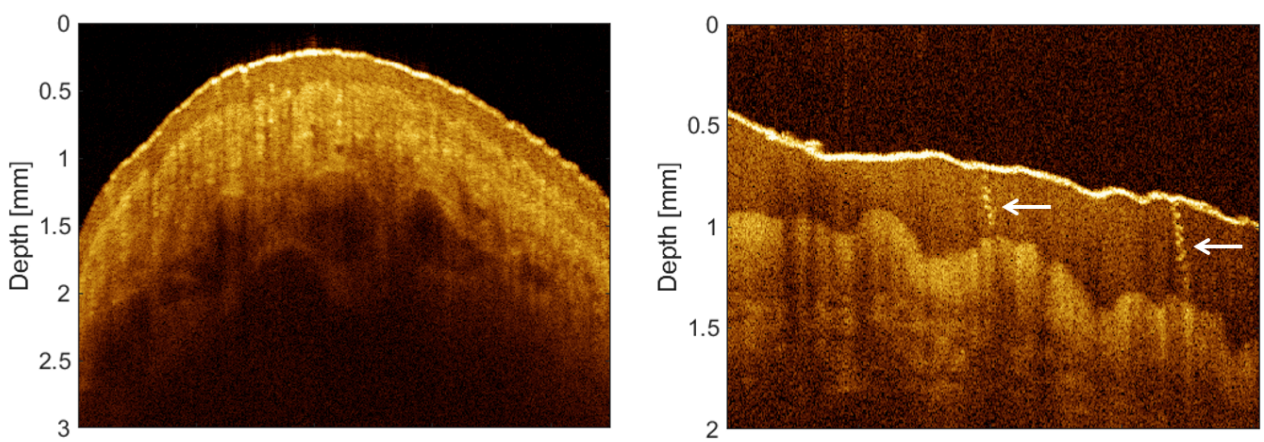

Figure 7. (Left) Seven averaged B-scans produced this speckle-reduced fingertip image. The sweep speed was 100 kHz. (Right) Three averaged B-scans at different planes to capture the sweat duct spirals (arrows). The pitch of the spirals is about 50 μm.

3. OCT PERFORMANCE

A shot-noise-limited sensitivity of 107 dB for 1.9 mW sample power was obtained as shown in Fig. 6. These measurements were performed using a 40 kHz sweep and direct hardware clocking. Similar shot-noise-limited performance is anticipated at other sweep rates as well.

Low noise allowed deep penetration in the fingertip image of Fig. 7(left). Axial resolution of 8.2 μm (6.3 μm in tissue) was estimated in Fig. 7(right) with a 62 nm data collection window by digitally compensating for

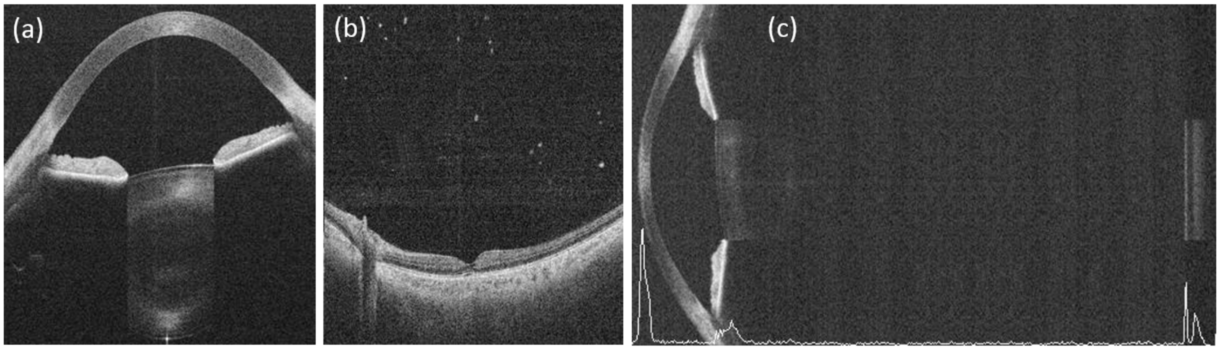

Figure 8. Ophthalmic images taken with a 50 kHz sweep speed. (a) Anterior segment. (b) Retina. The spots in the aqueous region are due to the patient's asteroid hyalosis condition. (c) Full-eye biometry scan.

the laser power variation vs. wavelength to effectively flatten the spectrum, and then applying a multiwindow signal processing technique[9] to simultaneously achieve high resolution and low sidelobe levels at the expense of increased computation. Our version of this method takes the minimum signal from a series of images computed with Kaiser-Bessel windows of β values between 1 and 12. This results in a resolution close to that of a full-width rectangular window.

Ophthalmic images at a 50 kHz sweep rate are shown in Fig. 8 illustrating the flexibility of the VCSEL system made possible by low noise and long coherence length.

4. LIDAR APPLICATIONS

The VCSEL's long coherence length makes LiDAR applications possible. Frequency domain LiDAR is essentially swept source OCT at long range.[10,11]

The VCSEL engine was run at 500 sweeps/sec for LiDAR and distributed sensing applications. The tuning range was > 50 nm and the optical power peaked out at ~ 50 mW. The main reason for the low sweep rate is to keep the interference signal frequencies manageable given the large depths involved. The Nyquist depth at this sweep rate is around 14 meters when sampling at 2 GS/s.

A fiber interferometer was constructed where the sample arm was terminated in an FC/APC connector. The fibers were cut to minimize Rayleigh scattering signals from infringing on the imaging depths. A -67 dB reference reflection from a collimator/attenuator/mirror was put in place and 100 A-scans were averaged as shown in Fig. 9. From that, a -125 dB sensitivity was measured, 8 dB short of the calculated shot-noise limit. The trace

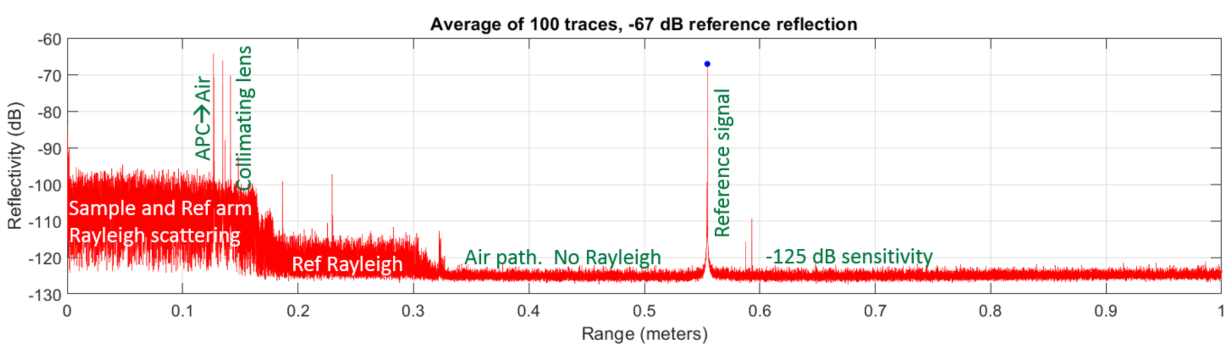

Figure 9. Signal from a -67 dB reference reflection showing that the system sensitivity is -125 dB. The setup uses a collimated beam, neutral density filters and a return mirror. The reference polarization was adjusted for maximum signal. The trace is the average of 100 laser sweeps.

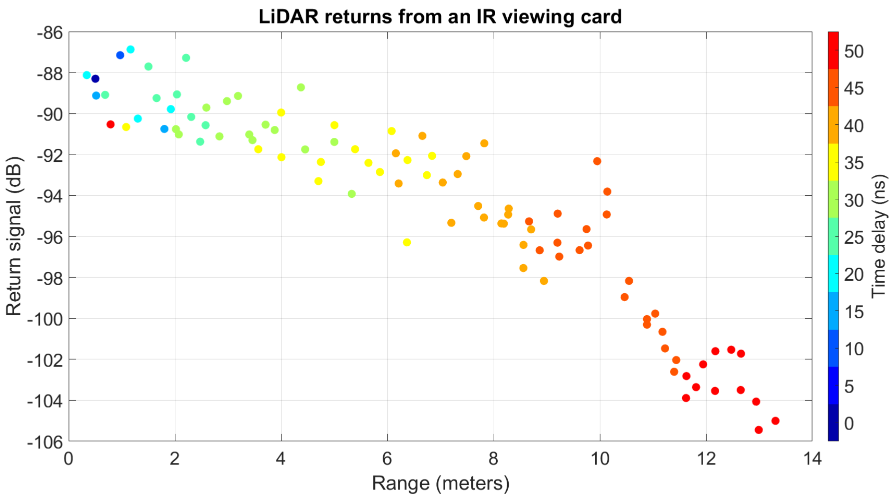

Figure 10. Free space LiDAR measurement using an IR viewing card as a target. Returns are processed with optimized signal processing time delays. The optimum delays, which are color coded, times the speed of light are roughly equal to the range.

shows the Rayleigh scattering from the sample and reference fiber arms of the interferometer. Having enough sensitivity to detect Rayleigh scattering in fibers is important for distributed temperature and strain sensing.

The coherence length of the VCSEL is a number that is often of interest. Generally, the question amounts to specifying the maximum imaging depth. The coherence length or alternately the linewidth is a difficult concept to discuss for swept source laser systems. Often, the term "instantaneous linewidth" is used to describe what is meant. Instantaneous does not mean zero time, but rather a short time interval over which the linewidth is computed. Then an additional question becomes what the relevant time interval is.

Delayed self-heterodyne linewidth measurements of MEMS tunable VCSELs show an increasing linewidth with optical delay until the linewidth saturates at a final value when all the mechanical Brownian motion is included in the measurement.[12] Generally the delay line must be longer than the coherence length of the source to make a proper measurement.[13] The concept gets complicated when linewidth reduction techniques are used.[14] This type of technique is used in OCT systems where an optical clock is used to measure the tuning rate of the laser. Such a system is effectively a linewidth reduction scheme since the VCSEL membrane vibration is measured as part of the overall tuning rate. To the extent that tuning jitter is calibrated out in a feed-forward

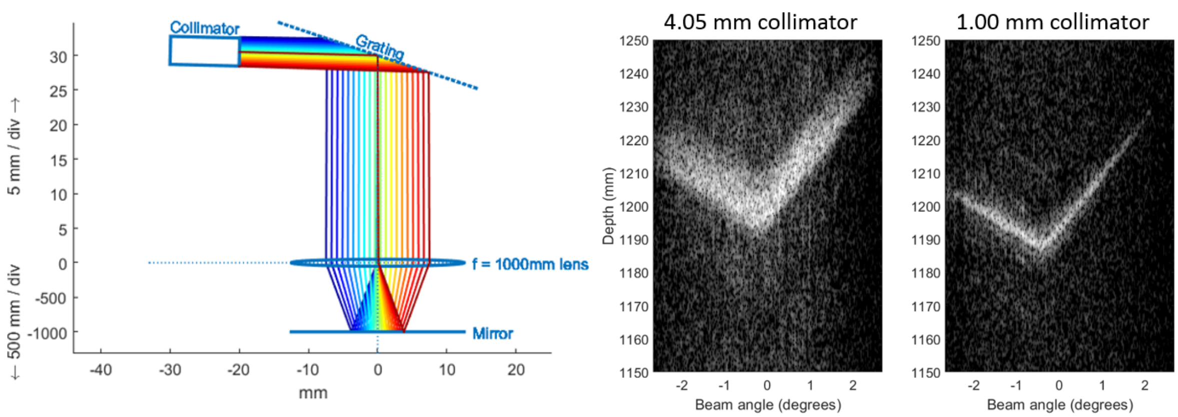

Figure 11. (Left) Ray trace of LiDAR grating head. Note the change in scale on the y-axis. (Center and Right) Images of a cardboard box corner for two different collimator aperture sizes.

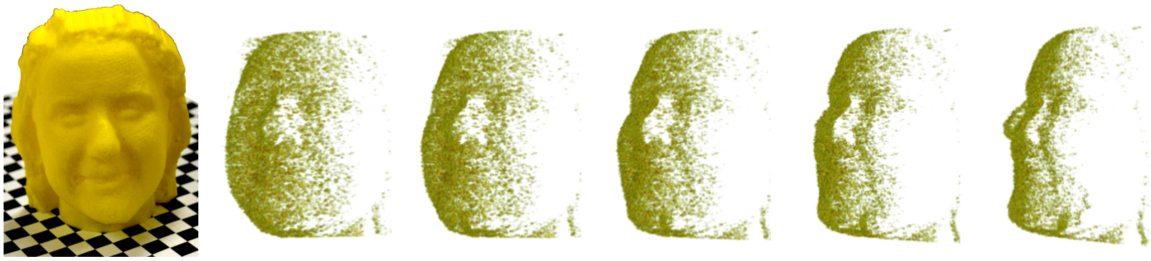

Figure 12. (Left) Photograph of a 3D printed head on a background 1-cm square checkerboard. (Right) Point clouds of the 3D printed head at 1-meter range obtained by a grating scan in one dimension and a galvo scan in the other.

fashion, those low frequency components should not be included in the "instantaneous" linewidth or alternately, the effective coherence length of the laser.

We estimate the linewidth due to Browian motion to be 110 MHz for a MEMS spring constant of k_m=500 N/m and FSR=21000 GHz from the following expression.[15,16]

$$\Delta\nu_{RMS} = \frac{2\ FSR}{\lambda}\sqrt{\frac{k_B T}{k_m}} \tag{1}$$

Electrical MEMS drive noise and radiation pressure[15] provide other forces on the MEMS membrane that might increase the linewidth. The 110 MHz figure corresponds to a coherence length of approximately 0.44 $c/\Delta\nu =$ 1.2 meters[17] assuming a Gaussian lineshape. An instantaneous coherence length, which sets aside Brownian motion, of 225 meters has been measured for a 1060 nm electrically-pumped MEMS VCSEL.[16]

A swept coherent LiDAR with careful clocking should be able to range beyond the Brownian coherence out to the instantaneous coherence. We constructed a LiDAR system with a 2000 mm optical path length clock interferometer and were able to achieve returns almost out to 14 meters (Fig. 10). This was for a free-space LiDAR where the sample beam was collimated and then focused by an f=10 m focal length lens. Some of the roll-off is due to the light-collection efficiency of the optical setup, however that component of the roll-off is fairly gentle. Most of the roll-off is due to a coherence limitation of the LiDAR system with careful clock compensation of the wavelength jitter from the Brownian motion and other noise sources. The signal time-delays at long range are considerable and must be compensated for digitally in the signal processing to reconstruct the full-amplitude point spread. The dots in Fig. 10 are color coded by this delay compensation to obtain the maximum point-spread amplitude. The optimal delay is $R/c - T_c$, where R is the range, c the speed of light and T_c is the time delay of the clock. This time delay in processing ensures maximum correlation between the signal and clock. In practice, it means that the signals need to be processed in blocks at different time delays to cover long ranges. In other words, processing time is increased since the signal needs to be digitally time delayed before the FFT and other processing to cover a deep band of ranges.

We have coupled frequency domain LiDAR with non-mechanical angular beam scanning by diffraction from a grating. There is a tradeoff between angular and depth resolution. The depth resolution sacrifice is acceptable in many LiDAR applications since OCT-type several-micron-level resolution is not required at long range. Traditional Fourier transform OCT processing is replaced with a Gabor transform and what would be an A-scan in OCT becomes a 2D image of range vs. angle. Investigating this scanning modality is important because a new generation of photonic integrated circuit (PIC) optical antennas work this way.[18,19] We have found that the practical range resolution in the experiment presented here is determined by time-dispersion in the grating head. We have calculated this by ray-tracing the grating scanner head (Fig. 11(left)). The mirror in the figure would be replaced with a scattering 3D object in a functional LiDAR. The resolution of cardboard box corner images scales with the collimator aperture size (Fig. 11(center, right)) and matches ray-trace calculations. Nevertheless, useful images of a small 3D printed face at 1 meter range have been obtained in Fig. 12 where one scan dimension is provided by the grating mechanism and the other by a galvo scanner.

5. DISTRIBUTED SENSING

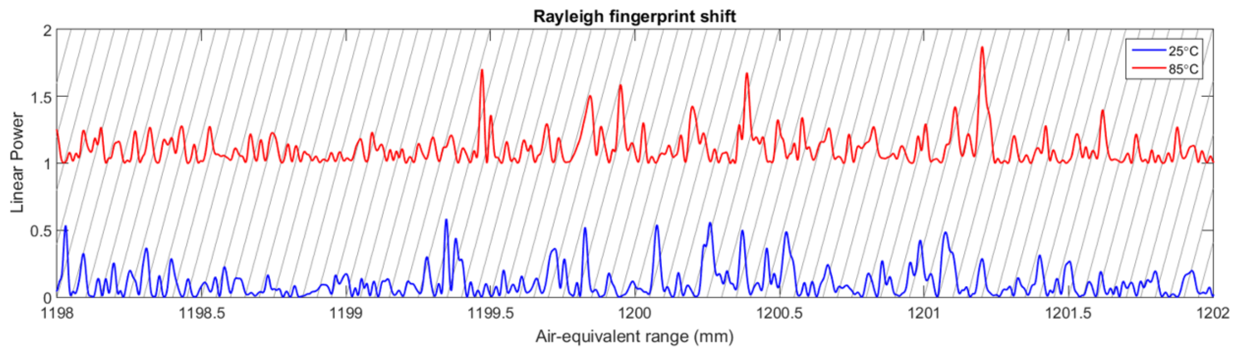

Figure 13. Rayleigh scattering "fingerprints" of a short section of fiber. These are LiDAR reflection measurements. Increasing the temperature of a preceding length of fiber from $25°C$ to $85°C$ moves the fingerprint by 0.124 mm due to thermal expansion and thermo-optic effects.

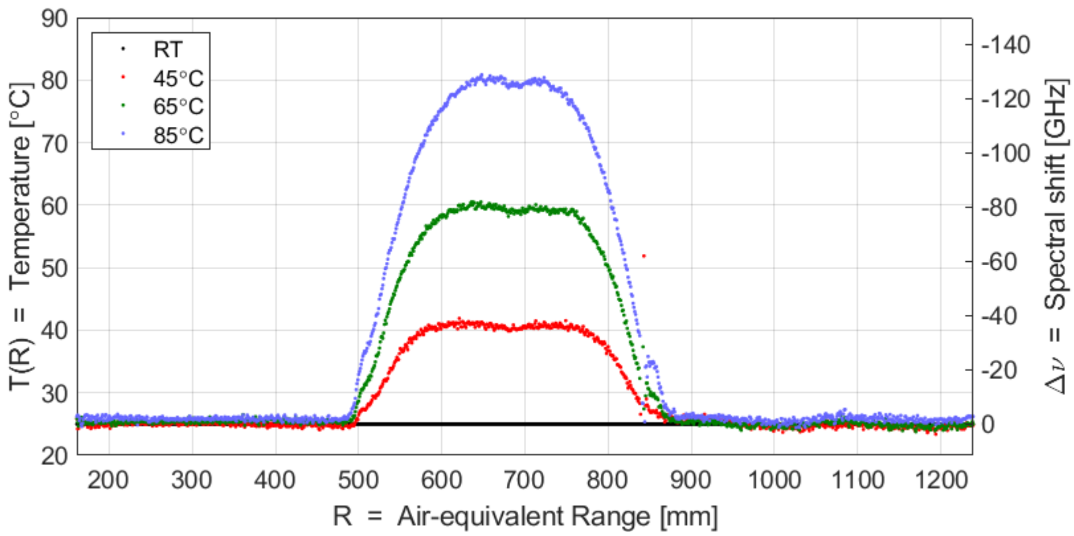

Figure 14. Distributed temperature sensing over a 1.2 meter length of fiber where the middle section was taped to a hot plate. The spectral shift of the Rayleigh fingerprint is measured and then converted to a temperature from fiber physical parameters.

The long coherence length of the VCSEL makes distributed strain and temperature sensing along an optical fiber possible with a LiDAR system.[20,21] The sensitivity needs to be high enough to clearly measure the Rayleigh scattering "fingerprint" of a fiber. Small, random index fluctuations in the optical fiber cause the Rayleigh scattering signal. It is not noise in the sense of being time dependent, but it is a fixed, random reflection pattern that is unique to each piece of fiber as shown in Fig. 13. The temperature of a preceding length of fiber was increased from $25°C$ to $85°C$ moving the fingerprint by 0.124 mm due to thermal expansion and thermo-optic effect. Cross-correlating the two fingerprints results in very accurate spatial shift measurements.

In addition to correlating Rayleigh fingerprints spatially, spectral correlation of Rayleigh fingerprints is useful.[20] The optical expansion and contraction of a fiber through strain and thermal effects can be measured this way. First, the spectrum is Fourier transformed into millimeter space and multiplied by a window, in this case ± 2 mm at the desired range, and transformed back to optical frequency space. The absolute value of the windowed spectra are then cross correlated to obtain $\Delta\nu$. The temperature shift is then:

$$\Delta T = \frac{\lambda}{c}\ \frac{1}{CTE + \frac{1}{n}\frac{dn}{dT}}\ \Delta\nu \tag{2}$$

We have demonstrated this with the VCSEL by measuring the temperature profile of an optical fiber whose mid-section was taped to a hot plate. Accurate distributed temperature vs. distance measurements can be made as demonstrated in Fig. 14. Strain measurements can be made through similar means. These measurements can also be made quite rapidly (hundreds to thousands of Hz) with with modest fiber lengths (few meters).

6. SUMMARY

A new optically-pumped MEMS tunable VCSEL structure has been demonstrated at 1060 nm where the strained InGaAs quantum well gain medium and semiconductor DBR are grown in the 1/2-VCSEL structure on a GaAs substrate. This is bonded to a silicon-based MEMS movable mirror structure that is electrically actuated to form a full tunable VCSEL. In addition, the VCSEL was co-packaged in a 14-pin butterfly package with a pump laser, dichroic mirror, isolator, and semiconductor optical amplifier (SOA). This results in a commercially interesting device with low noise, high sweep speeds, moderate tuning range, high power, and long coherence. High quality OCT images were demonstrated. LiDAR and distributed sensing experiments demonstrated useful ranging on the order of 10 meters. This is an isolated ranging result and should not be considered fundamental. There is room for further experimental and theoretical exploration of the coherence limit for MEMS-tunable VCSELs.

REFERENCES

[1] Lu, C., Waheed, N., Witkin, A., Baumal, C., Liu, J., Potsaid, B., Joseph, A., Jayaraman, V., Cable, A., Chan, K., Duker, J., and Fujimoto, J., "Microscope-integrated intraoperative ultrahigh-speed swept-source optical coherence tomography for widefield retinal and anterior segment imaging," *Ophthalmic Surgery, Lasers and Imaging Retina* **49**, 94–102 (2018).

[2] Choi, W., Potsaid, B., Jayaraman, V., Baumann, B., Grulkowski, I., Liu, J., Lu, C., Cable, A., Huang, D., Duker, J., and Fujimoto, J., "Phase-sensitive swept-source optical coherence tomography imaging of the human retina with a vertical cavity surface-emitting laser light source," *Optics Letters* **38**, 338–340 (2013).

[3] Knopp, K., Vakhshoori, D., Wang, P., Azimi, M., Jiang, M., Chen, P., Matsui, Y., McCallion, K., Baliga, A., Sakhitab, F., Letsch, M., Johnson, B., Huang, R., Jean, A., DeLargy, B., Pinzone, C., Fan, F., Liu, J., Lu, C., Zhou, J., Zhu, H., Gurjar, R., Tayebati, P., MacDaniel, D., Baorui, R., Waterson, R., and Van der Rhodes, G., "High power MEMs-tunable vertical-cavity surface-emitting lasers," in [*2001 Digest of LEOS Summer Topical Meetings*], **TuA1.3**, 31–32 (2001).

[4] Taira, K., Huber, R., Wojtkowski, M., and Fujimoto, J. G. Electronic communication of OCT images and system data collected with Coretek VCSEL to B.C. Johnson (May 2005).

[5] Flanders, D. C., Kuznetsov, M. E., Atia, W. A., and Johnson, B. C., "OCT system with bonded MEMS tunable mirror VCSEL swept source." US Patent application 2016/0329682 A1 (10 November 2016).

[6] Matsui, Y., Vakhshoori, D., Wang, P., Chen, P., Lu, C.-C., Jiang, M., Knopp, K., Burroughs, S., and Tayebati, P., "Complete polarization mode control of long-wavelength tunable vertical-cavity surface-emitting lasers over 65-nm tuning, up to 14-mw output power," *IEEE J. Quantum Electronics* **39**, 1037–1048 (2003).

[7] Orfanidis, S. J., "Multilayer structures," in [*Electromagnetic Waves and Antennas*], ch. 6, 186–240, Self published (2016). https://www.ece.rutgers.edu/ orfanidi/ewa/.

[8] Jayaraman, V., Jiang, J., Potsaid, B., Robertson, M., Heim, P. J. S., Burgner, C., John, D., Cole, G. D., Grulkowski, I., Fujimoto, J. G., Davis, A. M., and Cable, A. E., "VCSEL swept light sources," in [*Optical Coherence Tomography: Technology and Applications, Second Edition*], Drexler, W. and Fujimoto, J. G., eds., ch. 22, 659–686, Springer (2015).

[9] Chen, Y., Fingler, J., and Fraser, S. E., "Multi-shaping technique reduces sidelobe magnitude in optical coherence tomography," *Biomed. Opt. Express* **8**, 5267–5281 (Nov 2017).

[10] Wang, Z., Potsaid, B., Chen, L., Doerr, C., Lee, H.-C., Nielson, T., Jayaraman, V., Cable, A., Swanson, E., and Fujimoto, J., "Cubic meter volume optical coherence tomography," *Optica* **3**, 1496 (2016).

[11] Hariyama, T., Sandborn, P. A. M., Watanabe, M., and Wu, M. C., "High-accuracy range-sensing system based on FMCW using low-cost VCSEL," *Optics Express* **26**, 9285–9297 (2018).

[12] Yang, W., Rao, Y., Chase, C., Huang, M., and Chang-Hasnain, C., "Linewidth measurement of 1550 nm high contrast grating MEMS-VCSELs," in [*CLEO Technical Digest*], CF2F.4 (2013).

[13] Baney, D. and Sorin, W., "High resolution optical frequency analysis," in [*Fiber Optic Test and Measurement*], Derickson, D., ed., ch. 5, 179–202, Prentice Hall PTR (1998).

[14] Froggatt, M., Seeley, R. J., and Gifford, D. K., "High resolution interferometric optical frequency domain reflectometry (OFDR) beyond the laser coherence length." US Patent 7,515,276 (7 April 2009).

[15] Tucker, R., Baney, D., Sorin, W., and Flory, C., "Thermal noise and radiation pressure in MEMS Fabry-Perot tunable filters and lasers," *IEEE J. Selected Topics on Quantum Electronics* **8**, 88–97 (2002).

[16] John, D., Burgner, C., Potsaid, B., Robertson, M., Lee, B., Choi, W., Cable, A., Fujimoto, J., and Jayaraman, V., "Wideband electrically pumped 1050-nm MEMS-tunable VCSEL for ophthalmic imaging," *J. Lightwave Technology* **33**, 3461–3468 (2015).

[17] Yun, S. and Bouma, B., "Wavelength swept lasers," in [*Optical Coherence Tomography: Technology and Applications*], Drexler, W. and Fujimoto, J. G., eds., ch. 11, 362, Springer (2008).

[18] Poulton, C. V., Yaacobi, A., Cole, D. B., Byrd, M. J., Raval, M., Vermeulen, D., and Watts, M. R., "Coherent solid-state LIDAR with silicon photonic optical phased arrays," *Optics Letters* **42**, 4091–4094 (2017).

[19] Suni, P. J. M., Bowers, J., Coldren, L., and Yoo, S. J. B., "Photonic integrated circuits for coherent LiDAR," in [*18th Coherent Laser Radar Conference*], (2016).

[20] Froggatt, M. and Moore, J., "High-spatial-resolution distributed strain measurement in optical fiber with Rayleigh scatter," *Appl. Opt.* **37**, 1735–1740 (1998).

[21] Gifford, D., Kreger, S., Sang, A., Froggatt, M., Duncan, R., Wolfe, M., and Soller, B., "Swept-wavelength interferometric interrogation of fiber Rayleigh scatter for distributed sensing applications," in [*Proc. SPIE **6770**, Fiber Optic Sensors and Applications V*], 67700F (2007).